Long-term dynamics of bright bolides

L. Foschini[1], P. Farinella[2], Ch. Froeschlé[3], R. Gonczi[3], T.J. Jopek[4], and P. Michel[5]

[1] ISAO – CNR, Via Gobetti 101, 40129 Bologna, Italy
[2] Università di Trieste, Dipartimento di Astronomia, Via Tiepolo 11, 34131 Trieste, Italy
[3] Observatoire de la Côte d'Azur, Department Cassini, URA CNRS 1362, B.P. 229, 06304 Nice, France
[4] Obserwatorium Astronomiczne Uniwersytetu A. Mickiewicza, Sloneczna 36, 60–286 Poznań, Poland
[5] Osservatorio Astronomico di Torino, 10025 Pino Torinese (TO), Italy

Abstract. We have integrated backward and forward in time the orbits of 20 very bright bolides (with visual magnitude brighter than -10) over a time span of 5 Myr or more. The sample was mainly selected among events observed during the period between 1993 and 1996, but we have included also three older, particularly interesting events (Abee, 1952; Glanerbrug, 1990; and EN220991, 1991). For a large part of the sample, the orbit is known with sufficient accuracy from the reduction and analysis of photographic data. However, there are also some cases in which lower-accuracy orbital data were derived from other techniques, such as visual, seismic, and radar observation. For these events we have used two or three alternative initial orbits, consistent with the existing uncertainty. The results of our integrations show a great diversity of orbital evolution patterns, consistent with the behaviour of larger near-Earth objects. The most frequent fate (42% of the cases) is solar collision, followed by hyperbolic ejection (17%), and the average dynamical lifetime is of the order of 10 Myr. Three bolides either have initially or achieve later Aten-type or $Q < 1$ AU orbits, similar to the fraction of such objects in the near-Earth asteroid population. Only 2 bolides have a clear comet-like dynamical behaviour dominated by Jovian encounters, although ablation properties indicate that the fraction of very weak bolides is probably higher.

Key words: meteors, meteoroids – minor planets, asteroids – celestial mechanics, stellar dynamics – methods: numerical

1. Introduction

In the last decade, the complex of interplanetary solid bodies which populate the near-Earth part of the Solar System and can collide with our planet has attracted considerable attention from planetary scientists, dynamicists, meteoriticists and even geologists. These bodies range in size from micrometric particles to multi-km asteroids/comets and have a variety of chemical, physical and dynamical properties. The genetic relationships among the subpopulations observed (with different techniques) at different sizes and with the presumed source populations are very complex, and so are the main dynamical and collisional

Send offprint requests to: P. Farinella (paolof@dm.unipi.it)

evolutionary mechanisms at work. In particular, our knowledge is very limited in the 0.1–10 m size range, because the corresponding bodies are too small to be detected in space by astronomical techniques, and at the same time are so rare that they do not hit the Earth frequently enough to provide us with large data samples for statistical work. Only recently, observations from space-based optical sensors have provided relevant information about their flux into the high atmosphere (Tagliaferri et al. 1994). Yet, these bodies are very important, because they frequently deliver meteorites to the Earth's surface, and the relationship between meteorites and their parent asteroids is an outstanding scientific issue under rapid development. For instance, it has been recently pointed out (Farinella et al. 1998; Vokrouhlický & Farinella 1998) that for these small bodies a subtle non-gravitational force (the so-called *Yarkovsky effect*) may provide significant semimajor axis mobility in the main belt, making more efficient their transport into the resonant "escape hatches" which eventually deliver them to near-Earth space (for a recent detailed discussion of the relevant data and their implications, see Morbidelli & Gladman 1998).

Some five years ago, we first tackled the dynamical side of this problem, by studying numerically the long-term orbital evolution of 17 very bright bolides, mostly ranging in size between 1 and 10 m and including the four ones observed photographically and associated with recovered meteorite falls (Jopek et al. 1995). The most important conclusion of that paper was that the main dynamical mechanisms and evolutionary patterns were fairly similar to those previously found for sizeable near-Earth objects, suggesting common sources for the two populations. Only 2/17 bodies had comet-like orbits undergoing close encounters with Jupiter, indicating a minor but non-negligible cometary component. This was in agreement with earlier results on the orbits of sporadic photographic meteors (e.g., Whipple 1938) and with a variety of other arguments and observations (Binzel et al. 1992). The four meteorite-delivering, photographically observed bodies (all ordinary chondrites) had all dynamical behaviours consistent with an origin in the inner part of the asteroid belt.

A critical aspect of this kind of work is the fact that only for a small fraction of the observed bolides data are available of sufficient quantity and quality to allow a reliable determi-

Table 1. Catalogue of bolides in chronological order (orbital elements given in the 2000.0 heliocentric ecliptic reference system). The question mark in the Type column indicates large uncertainty in the classification.

Bolide	Apparition Time (UT)	a [AU]	e	q [AU]	ω [deg]	Ω [deg]	i [deg]	Mass [kg]	Type
1 Abee[a] 1	1952 06 10 06:05	1.9	0.49	0.96	326	260.0	1.3	107	E4
2 Abee[a] 2	1952 06 10 06:05	2.4	0.6	0.95	327	260.0	0.5	107	E4
3 Glanerbrug[b] 1	1990 04 07 18:32:38	3.3	0.7	0.90	220	17.8	25	20–200	L–LL
4 Glanerbrug[b] 2	1990 04 07 18:32:38	1.9	0.5	0.91	223	17.8	22	20–200	L–LL
5 EN220991[c]	1991 09 22 16:47:30	0.75	0.38	0.47	18	179.3	19	–	I(?)
6 Lugo[d] 1	1993 01 19 00:33:29	0.58	0.75	0.14	171	119.0	45	–	I–II(?)
7 Lugo[e] 2	1993 01 19 00:33:29	0.65	0.51	0.3	179	119.0	24	4×10^5	II
8 Meuse[f]	1993 02 22 22:12:45	1.50	0.567	0.651	266.9	334.4071	32.6	3000	I
9 Polná[f]	1993 08 07 21:08:15	2.003	0.5162	0.9691	209.52	135.4415	18.90	37.7	I
10 Marshall Isl.[g] 1	1994 02 01 22:38:09	1.73	0.66	0.59	269	132.92	2	1.6×10^6	I
11 Marshall Isl.[g] 2	1994 02 01 22:38:09	2.1	0.74	0.56	268	132.92	2	1.6×10^6	I
12 Dresden[f]	1994 02 15 23:06:23	2.338	0.5783	0.9859	173.90	327.1296	33.841	12.9	I
13 Ulm[f]	1994 05 25 21:28	2.04	0.560	0.8978	313.1	244.5262	2.50	500	IIIA
14 St. Roberts[h]	1994 06 15 00:02	1.9	0.48	1.0158	179	83.764	0.7	1500	H5
15 Kouřim[f]	1995 04 22 22:28:40	2.374	0.7878	0.5039	277.58	32.3858	4.119	109	I
16 Žamberk[f]	1995 08 04 01:17:38	1.616	0.7508	0.4026	113.98	311.2971	3.99	2.9	IIIB
17 Odra[f]	1995 10 24 21:01	1.327	0.571	0.569	280.2	211.0381	52.8	39	I
18 Tisza[f]	1995 10 25 02:25:53	1.077	0.8067	0.208	140.4	31.2595	6.2	890	I
19 EN081195B[f]	1995 11 08 20:39	2.2	0.83	0.39	110	46.021	5.4	2.4	IIIB
20 Hradec[f]	1995 11 23 01:29	3.39	0.779	0.749	243.3	240.3362	11.99	3600	I
21 Ózd[f]	1996 01 16 20:54:00	2.859	0.6626	0.9644	198.04	295.3652	35.94	9.7	I
22 Dobříš II[f]	1996 03 15 19:24:36	7.2	0.88	0.892	141.2	355.5530	8.3	620	II
23 EN270796[i]	1996 07 27 00:16:02	6.49	0.9182	0.5310	269.82	124.2953	7.16	13.5	IIIB
24 Honduras[l] 1	1996 11 23 04:05	1.1	0.09	0.98	329	61.2	7	2×10^4	I(?)
25 Honduras[l] 2	1996 11 23 04:05	1.5	0.33	0.997	358	61.2	16	2×10^4	I(?)
26 Honduras[l] 3	1996 11 23 04:05	2.2	0.56	0.99	4	61.2	21	2×10^4	I(?)

[a] Calculated from data in Griffin et al. (1992). Meteorite recovered. Here the mass indicated is the mass of the meteorite.

[b] Calculated from data in Jenniskens et al. (1992). Meteorite recovered.

[c] Borovička & Spurný (1998). Probable meteorite fall.

[d] Calculated from data in Cevolani et al. (1993, 1994).

[e] Calculated from data in Foschini (1998).

[f] Spurný (1997). Probable meteorite fall. For bolides 18 (Tisza) and 20 (Hradec)

[g] Tagliaferri et al. (1995).

[h] Brown et al. (1996). Meteorite recovered.

[i] Spurný & Borovička (1997).

[l] Calculated from data in Borovička et al. (1999).

nation of pre-atmospheric entry orbital elements, from which initial conditions for the long-term orbital integrations can be calculated. On the other hand, it is clear that the statistical robustness of any conclusion we may draw from the integrations depends on having analysed a sufficiently numerous and representative sample of bodies. Thus, we have now carried out a thorough search in the available literature to identify all the other bright bolides for which orbital data are available or can be derived. As we shall see in Sect. 2, we have now identified 20 more such bodies, mostly appeared in the time interval between 1993 and 1996 and reaching at least visual magnitude −10, with inferred sizes ranging from about 0.1 to 10 m. After analysing the distribution of the corresponding orbital parameters (Sect. 3), we have derived initial conditions for the integrations with the same methods discussed in Jopek et al. (1995), as summarized in Sect. 4 below. Then, we have integrated these orbits over a longer time span than we had done in 1995 (at least

10 Myr), thanks to the increased computing speed which is currently available. The results of these integrations are discussed in Sect. 5, and the main conclusions and some remaining open problems are summarized in Sect. 6.

2. Selection of data

After an extensive search in the literature, we have chosen a new sample of 20 bolides, all having magnitudes brighter than −10. The orbital parameters and estimated masses of these bodies are listed in Table 1, where the corresponding references are also indicated. In a first stage we have restricted ourselves to the time window from 1993 to 1996, but later on we decided to include also three older interesting bolides (Abee, Glanerbrug and EN220991), which had appeared in 1952, 1990, and 1991, respectively. We recall that the Abee and Glanerbrug bolides were associated with meteorite falls, in both cases fairly rare

Table 2. The input data used for the recalculation of the orbital elements of four bolides. The azimuth and elevation are the horizontal coordinates of the radiant point. The azimuth is measured clockwise from the North point on the horizon. All information comes from the sources quoted in Table 1.

Bolide	Apparition Time (UT)	Longitude [deg]	Latitude [deg]	Azimuth [deg]	Elevation [deg]	V [km s^{-1}]
1	1952 06 10 06:05 $\pm$ 1	-113.01 ± 0.01	54.22 ± 0.01	300 ± 10	18 ± 5	14 ± 2
2	1952 06 10 06:05 $\pm$ 1	-113.01 ± 0.01	54.22 ± 0.01	300 ± 10	18 ± 5	15 ± 2
3	1990 04 07 18:32:38 $\pm$ 1	$+6.95 \pm 0.01$	52.22 ± 0.01	60 ± 7	41 ± 6	23 ± 4
4	1990 04 07 18:32:38 $\pm$ 1	$+6.95 \pm 0.01$	52.22 ± 0.01	60 ± 7	41 ± 6	20 ± 4
6	1993 01 19 00:33:29 $\pm$ 1	$+11.91 \pm 0.01$	44.48 ± 0.01	146.5 ± 0.5	14 ± 5	26 ± 4
7	1993 01 19 00:33:29 $\pm$ 1	$+11.91 \pm 0.01$	44.48 ± 0.01	146.5 ± 0.5	5.0 ± 0.3	18 ± 3
24	1996 11 23 04:05 $\pm$ 5	-88.87 ± 0.03	15.28 ± 0.03	177 ± 10	19 ± 5	12.0 ± 0.7
25	1996 11 23 04:05 $\pm$ 5	-88.87 ± 0.03	15.28 ± 0.03	177 ± 10	19 ± 5	15 ± 1
26	1996 11 23 04:05 $\pm$ 5	-88.87 ± 0.03	15.28 ± 0.03	177 ± 10	19 ± 5	18 ± 1

types of material. The Abee meteorite, an E4 enstatite chondrite, is of particular interest owing to the relationship between this type of meteorites and a particular source region in the main asteroid belt (Gaffey et al. 1992, Farinella et al. 1994). The Glanerbrug meteorite, which penetrated the roof of a house, was a rare inhomogenous kind of chondrite, with darker and lighter breccias, classified as LL and L chondrites respectively, within a fine-grained matrix (Jenniskens et al. 1992).

Note that most orbits in our list have been derived by means of data obtained from the photographic technique (Spurný 1997, Spurný & Borovička 1997). In these cases, it is possible to calculate with good precision the orbit of the meteoroid, by means of the gross-fragmentation model described by Ceplecha et al. (1993). It is worth noting that recently Ceplecha has improved the model, which can currently reach a precision of about 1 m along the atmospheric trajectory of the fireball (Ceplecha 1999).

The gross-fragmentation model allows one to calculate the ablation coefficient of the body and therefore to establish in a fairly reliable way some physical properties of the original meteoroid. According to the value of the ablation coefficient, Ceplecha & McCrosky (1976) classified meteoroids into four groups, as follows:

– I: stony
– II: carbonaceous chondritic
– IIIA: cometary
– IIIB: soft cometary

Later on, Ceplecha (1994) used the relatively abundant meteor data for sizes smaller than 1 m to draw some inferences about the poorly known meteoroid population in the 1–10 m size range. He concluded that carbonaceous bodies are the most common at 1 m size, whereas at 10 m the very weak IIIB-group cometary bodies are the dominant component. This was also recently confirmed by satellite observations (Ceplecha et al. 1997). As for our sample of bright bolides, in most cases we know the classification of either the delivered meteorites or the photographic fireballs, according to Ceplecha's methodology (see Table 1). Only for Lugo and Honduras there is some uncertainty, due to the limited available data. We will comment later on about the implications of this physical information; note, however, that Ceplecha's groups do not really refer to the

chemical-mineralogical composition of the bodies, but rather to their physical and structural properties. Whereas in the case of meteorites some comparisons are possible with laboratory measurements for different meteorite types, nobody does really know so far how a comet fragment would look like and interact with the atmosphere.

For some fireballs for which photographic data were not available, we have derived the orbital parameters from satellite observations (Brown et al. 1996, Tagliaferri et al. 1995), visual observations by occasional witnesses (Borovička et al. 1999, Cevolani et al. 1993, Griffin et al. 1992, Jenniskens et al. 1992), seismic records (Cevolani et al. 1994, Foschini 1998), or with a combination of these data and methods. In these cases, the orbital elements are quite difficult to calculate and in order to derive them it is necessary to adopt an interdisciplinary approach, based on concepts and methods from different disciplines, including hypersonic aerodynamics, physics of shock waves, optics, seismology and acoustics. Actually, in recent years several new theories on the aerodynamics of large meteoroids (i.e. larger than some meters) in the Earth's atmosphere have been proposed (e.g. Chyba et al. 1993, Hills & Goda 1993, Lyne et al. 1996), but all rely on a number of approximations and there is plenty of open problems (Ceplecha 1995), in particular when meteoroids of size of the order of 10 m are involved. Some possible solutions are being discussed in the current literature (e.g. Borovička et al. 1998a, 1998b, Foschini 1998, 1999), but there is still a clear need for both relevant data and improved theories and models.

Therefore, in order to take into account the large uncertainties which in some cases affect the derivation of the orbital elements, for several bolides (Abee, Glanerbrug, Lugo and Honduras) two or three alternative solutions have been recalculated from different sets of starting data, as indicated in Table 2. In another case (Marshall Islands) two solutions corresponding to different values of the bolide's velocity were already given in the original paper of Tagliaferri et al. (1995). For these five bodies, the two or three alternative sets of orbital parameters are listed separately in Table 1, and have been used in the following stage of our work to derive different sets of starting conditions for the numerical integrations. Thus, we have dealt with a total of 26 orbits, some of them corresponding to the same physical object.
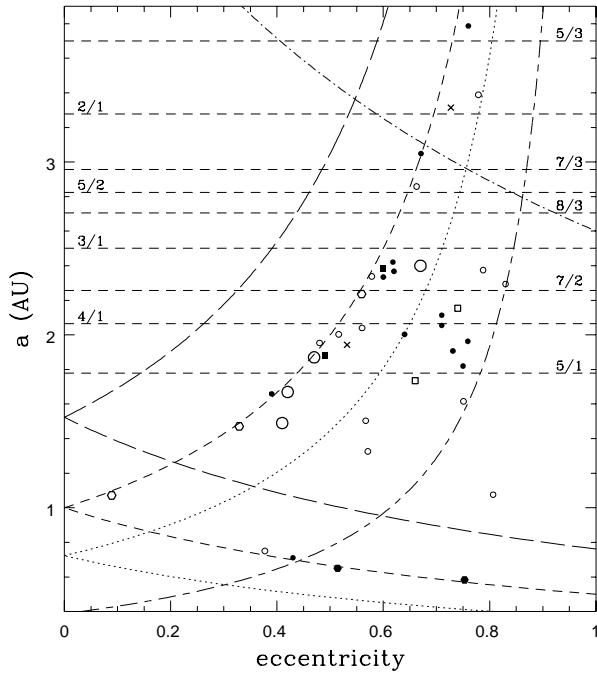
Fig. 1. The position in the orbital semimajor axis vs. eccentricity plane of the sample of orbits studied in this paper (small open circles, plus special symbols for the cases when we selected multiple sets of elements: Abee, full squares; Glanerbrug, crosses; Lugo, full hexagons; Marshall Islands, open squares) and for that of Jopek et al. 1995 (small full circles, plus large open circles for the four meteorite-delivering photographic fireballs Příbram, Lost City, Innisfree and Peekskill). Dashed and dotted curves correspond to orbits having perihelia and aphelia nearly tangent to the orbits of Mars, the Earth and Venus.
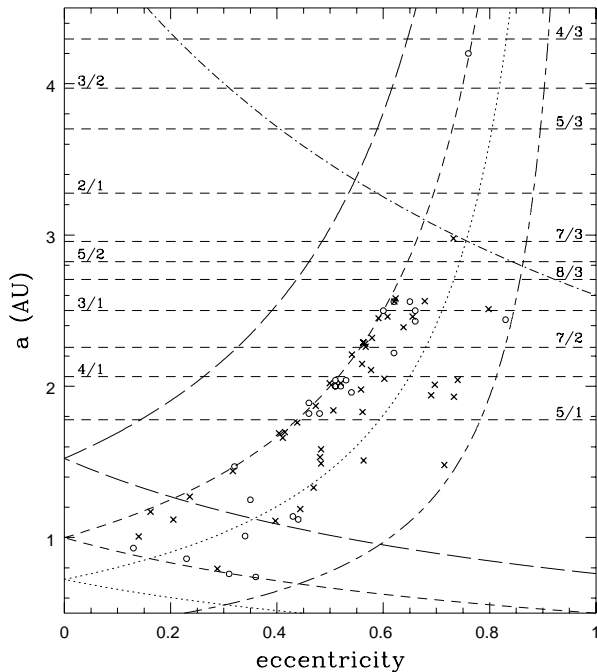

Fig. 2. The same as Fig. 1 but for the chondritic meteoroids listed by Wetherill & ReVelle (1981, open circles) and Halliday et al. (1996, crosses). These are the orbits discussed in the recent paper on the orbital distribution of meteoroids by Morbidelli & Gladman (1998).
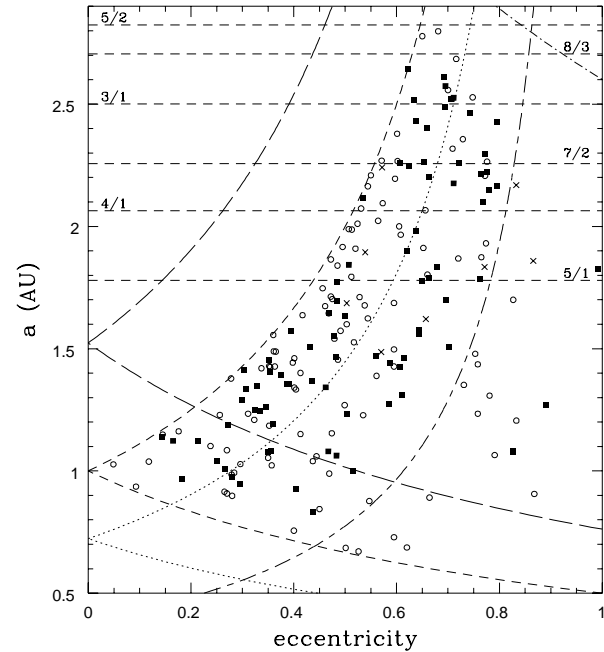

Fig. 3. The same as Fig. 1 but for the the currently known Earth-crossing asteroids. Open circles correspond to bodies less than 1 km in diameter, full squares to the 1 to 5 km diameter range and crosses to bodies larger than 5 km. This is a subset (Apollo and Aten asteroids only) of the sample of near-Earth asteroids with good quality orbits recently studied by Gladman et al. (1999). Diameters have been estimated from reasonable guesses of albedos (as explained in Migliorini et al. (1998) when this parameter has not been directly measured.

3. Distribution of current orbits

Before integrating the orbits listed in Table 1 over millions of years, it is worth making some comments on their distribution in the a–e plane, compared to those for both smaller and larger members of the Earth-crossing population. Fig. 1 shows this distribution for our current sample (small open circles, plus special symbols for those with uncertain orbits) and for that of Jopek et al. 1995 (small full circles, plus large open circles for the four meteorite-delivering photographic fireballs). This can be compared to the distributions for the smaller chondritic meteoroids (diameter of about 1–10 cm) listed by Wetherill & ReVelle (1981) and Halliday et al. (1996), as shown in Fig. 2, and to that for the currently known Earth-crossing (Apollo and Aten) asteroids with good quality orbits, divided into three different diameter ranges (Fig. 3).

It is interesting to note that, despite the greatly different selection effects involved in the observational methods used to collect these data, there is no striking difference in the overall appearance of the distributions. For instance, the abundance of Aten-type orbits with $a < 1$ AU is ≈ 5–10% for all the three samples. The fact that the bolides are somewhat more concentrated near the $q = 1$ AU line can be easily explained by the higher collision probability resulting from this orbital configuration (Wetherill 1967). Apart from this, the orbits look broadly scattered in the region of the a–e plane where collisions with the
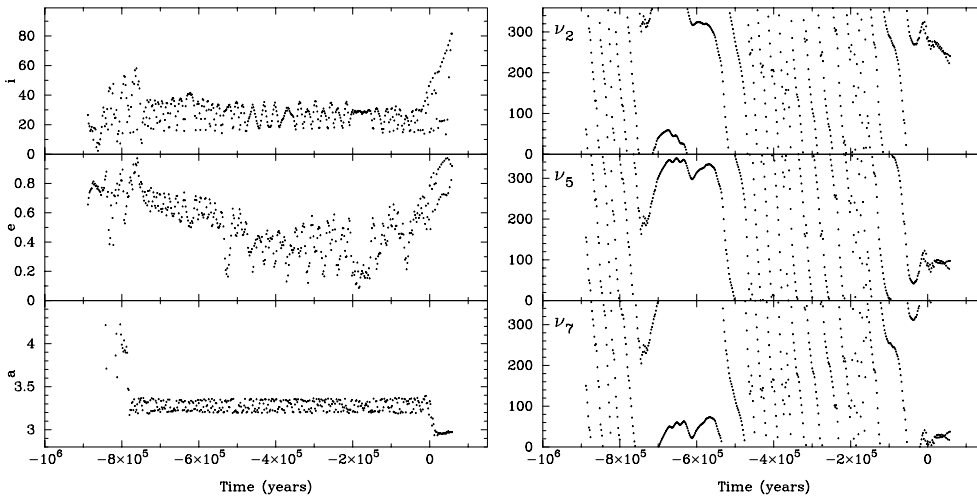
bolide 20 (Hradec)

Fig. 4. Orbital evolution of bolide 20 (Hradec) in the time span $-0.87 < t < 0.06$ Myr. The left-side panels show the semimajor axis a (AU), eccentricity e and inclination i (degrees) vs. time, whereas the right-side panels show the critical arguments for the ν_2, ν_5 and ν_7 secular resonances. Note that in the backward integration a is locked in the 2/1 mean motion resonance with Jupiter.

Earth are possible, with no strong clustering, e.g. near Jovian resonances; this indicates that most bolide orbits are already "dynamically evolved" when they hit the Earth, namely they have been scattered around by close planetary encounters after having been transported into near-Earth space.

Table 1 and Fig. 1 show that three of the four bolides classified in Ceplecha's IIIA and IIIB groups have orbits which are dynamically decoupled from Jupiter, i.e., they are not typically cometary orbits. In our opinion, there are two possible explanations for this, which do not necessarily exclude each other: (i) the asteroid belt may also deliver very weak, fragile and possibly porous bodies, as suggested for instance by the recently determined low density of C-type asteroid 253 Mathilde, encountered by the NEAR probe in June 1997 (Yeomans et al. 1997, Foschini 1998); (ii) the dynamical pathway between typical, Jupiter-coupled cometary orbits and "asteroidal" ones, such as those of comet P/Encke and the Taurid meteoroids (Valsecchi et al., 1995) is an important one, and quite many small bodies reach the Earth-crossing region through this *route*. Note, however, that neither cometary orbits nor comet-like physical properties account for a dominant fraction of our sample of bright bolides. At least in part, this is probably due to selection effects, as photographic observations have been preferentially reduced for bolides of types I and II, considered as more interesting because they are possibly associated to meteorites (Z. Ceplecha, private communication).

4. Calculation of the initial conditions

In this section we describe the procedure by which we have calculated the initial positions and velocities of the bolides, needed to numerically integrate their orbits. Tables 1 and 2 summarize all starting data; in Table 1 the number of significant digits is consistent with the expected accuracy (apart from the apparition times T_0, whose error is at most a few minutes). The errors in the orbital elements are caused by the limited accuracy of both the observations and the models used to reconstruct the trajectory

prior to atmospheric entry (the corresponding errors for the coordinates of the radiant points and the entry velocity are given in Table 2). In all cases, these errors are small enough that a qualitative dynamical study such as performed in this paper is meaningful.

To fulfil the requirements of our long-term integration software, the data reported in Table 1 had to be:

– complemented by the moment of perihelion passage;
– transformed into rectangular coordinates;
– integrated to a common initial epoch, in our case JD 2440000.5.

All these steps have been carried out by the same method as described in Jopek et al. (1995), to which we refer for further details. Following the first two steps, the rectangular coordinates of Table 3 give the state vectors of the orbits listed in Table 1. The corresponding final state vectors at the common osculating epoch JD2440000.5 and the equivalent set of the orbital elements are listed in Tables 4 and 5, respectively.

Since the orbital elements listed in Table 1 certainly include considerable observational and model errors, we may wonder whether the results of the numerical integration procedure are sensitive to any small change in the values of the initial state vectors. Therefore, exactly in the same way as in our earlier paper (Jopek et al. 1995), we have estimated the propagation of these uncertainties to our final values for the coordinates and velocities used as initial conditions for the long-term integrations. Table 6 shows the maximum differences between the final coordinates of the test particles corresponding to each bolide. In general, the sensitivity does not appear very strong: for most of the orbits the differences are of the order of 10^{-2} AU and 10^{-4} AU/day, i.e. much larger than the initial "noise", but small enough that the long-term integrations to be discussed in Sect. 5 can still be seen as representative for the real population of small bodies hitting the Earth. The largest instability appears to be associated with bodies nos. 4, 5, 10, 11, 19 and 25.

Table 3. Rectangular coordinates of 26 bolides in the 1950.0 heliocentric ecliptic reference frame. T_0 is the corresponding epoch in Ephemeris or TDT Julian days. x, y, z are given in AU, $\dot{x}, \dot{y}, \dot{z}$ in AU/day.

Bolide	T_0	x	y	z	$\dot{x}$	$\dot{y}$	$\dot{z}$
1	2434173.7538	-0.187936	-0.998401	0.000886	0.019166	-0.007618	0.000359
2	2434173.7538	-0.187125	-0.997923	0.000882	0.019736	-0.008326	0.000076
3	2447989.2733	-0.956893	-0.295762	0.004642	0.011791	-0.016715	-0.009122
4	2447989.2733	-0.956719	-0.295708	0.004641	0.010560	-0.016458	-0.007501
5	2448522.2003	1.003497	-0.023438	-0.004880	0.002792	0.012929	-0.004514
6	2449006.5239	-0.468862	0.867105	0.002265	-0.003563	-0.006481	0.006174
7	2449006.5239	-0.468172	0.865751	0.002298	-0.009614	-0.005481	0.004871
8	2449041.4262	-0.887811	0.437508	0.004326	0.002067	-0.017527	-0.009468
9	2449207.3814	0.714434	-0.719436	-0.003491	0.011230	0.016271	-0.006716
10	2449385.4438	-0.666574	0.733063	0.003259	-0.020418	-0.003066	0.000699
11	2449385.4438	-0.672908	0.740032	0.003290	-0.021220	-0.001879	0.000696
12	2449399.4635	-0.823728	0.545437	0.004017	-0.010725	-0.014574	-0.012044
13	2449498.3951	-0.445872	-0.909563	0.002142	0.015416	-0.014174	0.000801
14	2449518.5021	-0.121626	-1.008543	0.000564	0.020596	-0.002602	-0.000354
15	2449830.4373	-0.854930	-0.528961	0.004140	0.020553	-0.006328	-0.001267
16	2449933.5546	0.660901	-0.769560	-0.003232	0.001622	0.019916	0.000983
17	2450015.3764	0.857742	0.503189	-0.004154	-0.013886	0.003355	-0.012960
18	2450015.6020	0.854580	0.505775	-0.004139	-0.017789	0.001736	0.001233
19	2450030.3611	0.700012	0.709378	-0.003382	-0.021481	-0.001107	0.001477
20	2450044.5625	0.498032	0.852133	-0.002397	-0.022244	0.000976	-0.004071
21	2450099.3715	-0.411420	0.893499	0.002024	-0.015182	-0.010030	-0.012924
22	2450158.3095	-0.990815	0.088211	0.004817	-0.009277	-0.021422	-0.003188
23	2450291.5119	0.562841	-0.845407	-0.002758	0.005434	0.022427	-0.002156
24	2450410.6709	0.485372	0.859986	-0.002335	-0.015126	0.009421	0.002356
25	2450410.6709	0.485170	0.859630	-0.002334	-0.016619	0.009554	0.005559
26	2450410.6709	0.485109	0.859518	-0.002334	-0.017850	0.009437	0.007722

5. Long-term integrations and results

The dynamical evolution of the 20 bolides has been studied by integrating the 26 orbits listed in Table 5. We recall that for 5 bolides, two or three different sets of starting orbital elements have been determined (see Sect. 2). The integrations were carried out with a Bulirsch-Stoer variable step-size technique (Stoer & Bulirsch 1980), optimized for dealing accurately with planetary close encounters (cf. Michel et al. 1996a). The dynamical model included all the planets except Pluto and Mercury, with the mass of the latter added to that of the Sun. The integration interval spanned at least 5 Myr backward and forward in time, with a total timespan of 10 Myr (this was extended in some specific cases).

As discussed in several recent papers which deal with long-term integrations of planet-crossing bodies, the results of the numerical integrations cannot be seen as deterministic reconstructions or predictions of the real evolutions. Nevertheless, they are very useful to provide qualitative and/or statistical information on the most common patterns of the orbital behaviours as well as on the efficiency of different dynamical mechanisms and the corresponding lifetimes. Integrating backward and forward in time just provides a simple way of doubling the size of the sample and thus of improving the statistics (note that backward integrations cannot provide information on the sources of the bodies, neither individually nor statistically). We will first consider all the bodies which either have a collision with the Sun or are ejected from the Solar System, and discuss separately the backward and forward integrations. Then, we will describe the evolutions of bodies strongly affected by planetary close approaches. The main results of our integrations are summarized in Table 7.

5.1. Backward integrations

A collision with the Sun is recorded for 10 orbits, whereas 4 others are ejected outside Saturn's orbit. Half of these 14 orbits have dynamical lifetimes shorter than 1 Myr (among them 4 collide into the Sun and 3 are ejected).

The $5/2$ and $2/1$ Jovian mean motion resonances are responsible for the ejection of 2 bolides: Abee-1 (1) and Hradec (20) (Fig. 4), respectively. As for Abee-1 (1), a close encounter with the Earth at time $t = -0.83\,\mathrm{Myr}$ (see Table 7) injects it into the $5/2$ resonance, which increases its eccentricity from 0.2 to 0.9. As a consequence, the body gets close to Jupiter's perihelion distance and eventually an approach to this planet ejects it out of Saturn's orbit.

The Hradec bolide (20) is located in the $2/1$ resonance during almost all its backward evolution. It is also temporarily located in the ν_2, ν_5 and ν_7 secular resonances (these are resonances betweeen the average precession rate of the perihelion longitude of the body and the corresponding eigenfrequencies

Table 4. Rectangular coordinates of the 26 bolides at the common epoch JD 2440000.5. Reference frame: barycentric, ecliptic 1950.0 (x, y, z in AU; $\dot{x}$, $\dot{y}$, $\dot{z}$ in AU/day).

Bolide	x	y	z	$\dot{x}$	$\dot{y}$	$\dot{z}$
1	1.99139	-0.29812	0.04509	0.0071563	0.0092862	0.0001161
2	3.14558	1.56525	0.02268	-0.0002181	0.0067250	-0.0000150
3	3.88990	3.75030	1.11995	-0.0015125	0.0036045	0.0018173
4	-1.11577	0.99928	0.51196	-0.0036182	-0.0136050	-0.0047204
5	0.94894	0.38301	-0.14076	-0.0061714	0.0113020	-0.0038700
6	-0.06241	0.76977	-0.30401	-0.0089166	0.0108546	0.0026510
7	-0.43268	0.88053	-0.01582	-0.0100802	-0.0046206	0.0048199
8	0.97383	1.73228	1.26872	-0.0065253	0.0034276	0.0001326
9	0.40948	1.31015	-0.41818	-0.0114388	0.0115704	-0.0000371
10	-0.20530	-1.90245	0.05025	0.0097024	0.0067037	-0.0004077
11	0.18177	-1.65020	0.03513	0.0090425	0.0117320	-0.0005117
12	2.36032	0.10917	0.92989	-0.0072707	0.0072176	0.0013587
13	1.15715	-1.39180	0.07010	0.0134222	0.0015432	0.0004952
14	0.73613	2.77504	-0.00504	-0.0068947	0.0026504	0.0000875
15	-3.05131	2.56822	0.27650	-0.0006735	-0.0048417	-0.0002488
16	-0.38767	-2.48547	-0.13454	0.0063418	0.0033938	0.0004841
17	0.40991	0.51717	-0.31791	-0.0214850	-0.0032302	-0.0106723
18	1.66403	-0.63360	-0.15097	0.0065013	0.0038437	-0.0000043
19	0.03578	-1.12858	-0.07465	0.0132318	-0.0146986	-0.0018491
20	3.24106	-4.83098	1.19030	0.0024488	0.0021883	0.0003334
21	1.22250	-3.72844	-0.34973	0.0055320	-0.0026646	0.0028734
22	10.61538	-8.07003	-1.03283	-0.0000996	0.0021681	0.0003122
23	-8.91604	-3.55505	1.09457	-0.0024542	-0.0028599	0.0004573
24	-1.07049	0.32254	0.14038	-0.0055908	-0.0146761	-0.0002922
25	0.24821	0.96401	0.07426	-0.0181670	0.0057394	0.0053230
26	-1.65793	-3.06146	-0.01621	0.0048624	-0.0030310	-0.0021723

for the secular evolution of the planetary perihelia). The presence of secular resonances inside the $2/1$ mean motion resonance is a well-known source of chaotic motion (Morbidelli & Moons 1993, Moons & Morbidelli 1995). As a consequence, the eccentricity is eventually pumped up to 0.98. Then a close encounter with Jupiter extracts the orbit from the resonance and the bolid is rapidly ejected from the solar system.

The Dobříš II (22) and EN270796 (23) bolides have both semimajor axes larger than that of Jupiter, high eccentricities and low orbital inclinations (see Tables 1 and 5). These orbits are very similar to those of many Jupiter-family comets; being close to the orbital plane of the planets, they undergo frequent close encounters with Jupiter. Thus, a close approach to Jupiter ejects them from the Solar System after only 0.1 and 0.04 Myr, respectively.

Different dynamical mechanisms are at the origin of the recorded solar collisions, depending on the starting locations of the small bodies. When the orbits have a semimajor axis $a > 2$ AU, the dynamical mechanisms responsible for the collision against the Sun are those described for the first time by Farinella et al. (1994):

– the ν_6 secular resonance (for bolides 13-Ulm and 19-EN081195B),
– the $3/1$ mean motion resonance with Jupiter (bolides Abee-2 (2) and Polná (9)),

– the overlapping of secular resonances inside mean motion ones (bolides nos. 3-Glanerbrug-1, 21-Ózd, 15-Kouřim and 26-Honduras-3). For instance, bolide 3-Glanerbrug-1 is located in the $2/1$ resonance with Jupiter and also in the Kozai resonance, its argument of perihelion ω librating around $90°$ (Fig. 5). Bolide Ózd (21), while being in the $5/2$ resonance with Jupiter, between $t = -0.10$ Myr and $t = +0.20$ Myr is also affected by the ν_3 and ν_4 secular resonances (involving the average precession rates of the perihelion longitude of the Earth and Mars); from $t = -0.19$ Myr to $t = 0.0$ Myr, the orbit is then in ν_2, ν_5, and ν_7. Note that the location of secular resonances involving the orbital frequencies of the terrestrial planets has been determined only recently (Michel 1997). Here we observe for the first time, for a body with $a > 2$ AU, the occurence and effect of the overlapping of a mean motion resonance with the ν_3, ν_4 and ν_2 secular resonances. Finally, during the interval $-2.46 \leq t \leq -2.20$ Myr bolide Kouřim (15) is located in the $4/1$ mean motion resonance as well as in the ν_2 and ν_5 secular resonances; Honduras-3 (26) is also located in these three resonances, but during the timespan $-5.01 \leq t \leq -4.7$ Myr.

Marshall Islands-1 (orbit 10) over about 0.5 Myr is located in the overlapping region of the ν_3 and ν_4 resonances. Such overlapping of two secular resonances with the terrestrial planets (here, the Earth and Mars) has been already analyzed by Michel
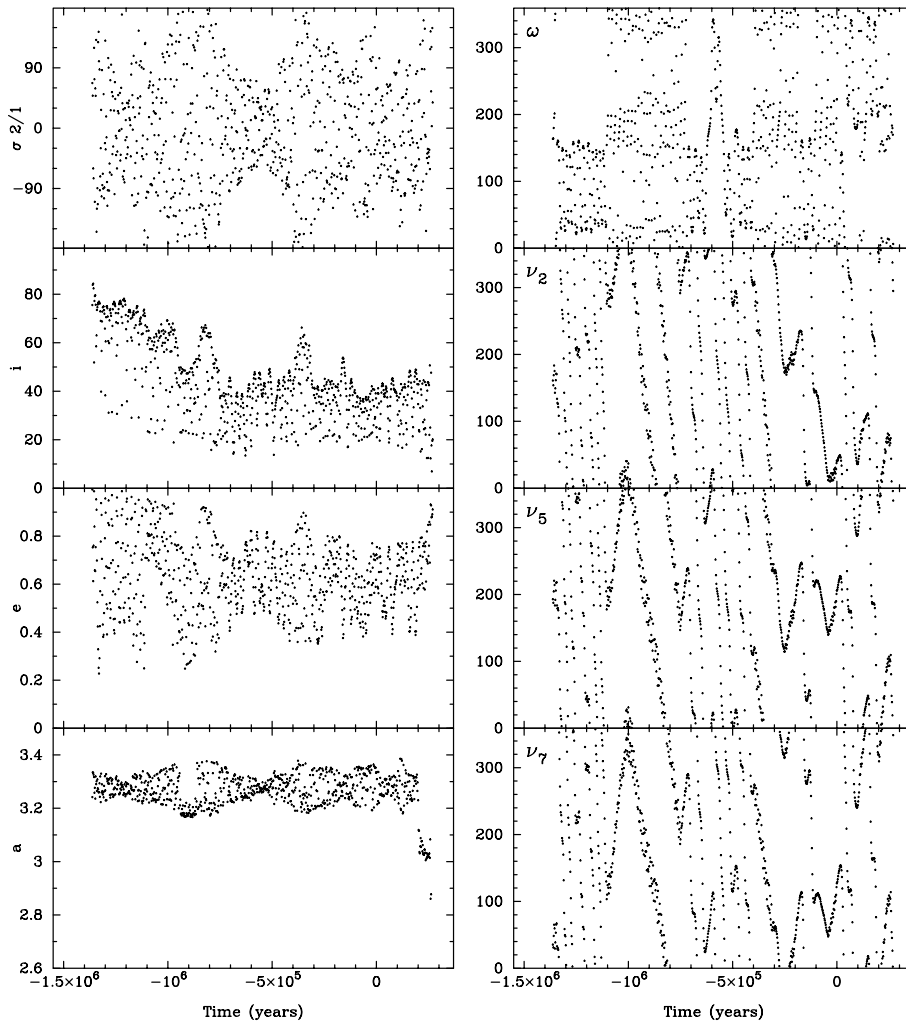
bolide 3 (Glanerburg-1)

Fig. 5. Orbital evolution of bolide 3 (Glanerbrug-1) in the time span $-1.36 < t < 0.27$ Myr. The left-side panels show the semimajor axis a (AU), eccentricity e, inclination i (degrees) and the critical argument of the 2/1 Jovian mean motion resonance, whereas the right-side panels show the critical arguments for the ν_2, ν_5 and ν_7 secular resonances plus, on the top, the body's argument of perihelion ω, which shows episodes of libration around $90°$ due to capture into the Kozai resonance. This orbits is almost always locked in the 2/1 mean motion resonance with Jupiter.
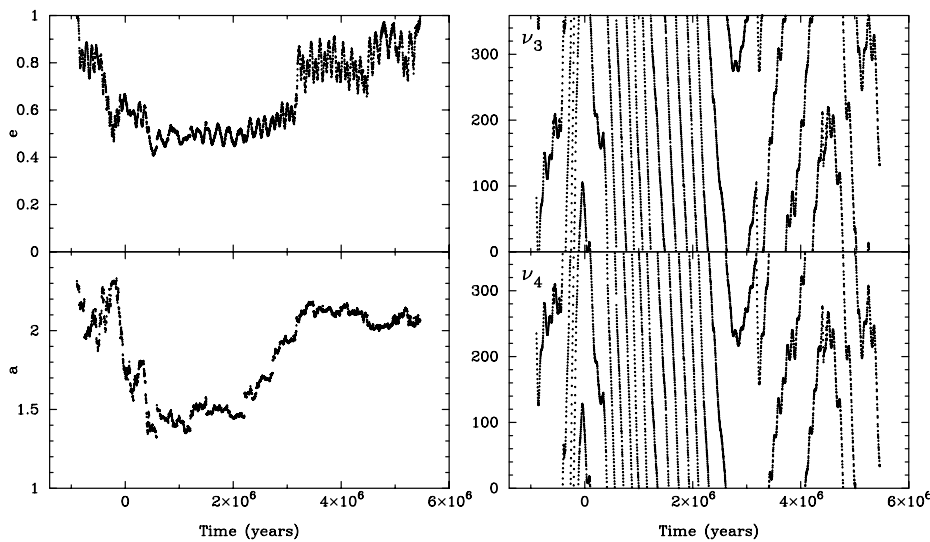
bolide 10 (Marshall Islands−1)

Fig. 6. Orbital evolution of bolide 10 (Marshall Islands-1) in the time span $-0.90 < t < 5.47$ Myr. The left-side panels show the semimajor axis a (AU) and eccentricity e vs. time, whereas the right-side panels show the critical arguments for the ν_3 and ν_4 secular resonances. Note that e reaches unity when the orbit is affected by these secular resonances with the Earth and Mars.
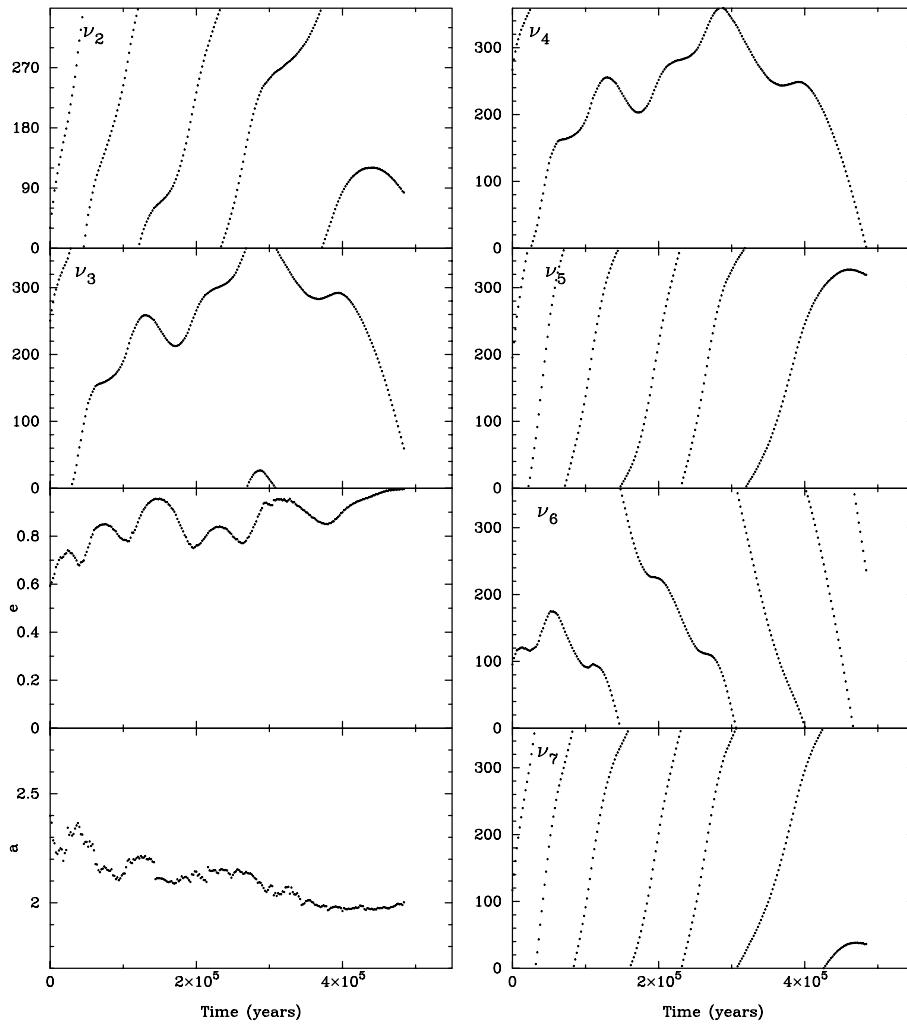
bolide 2 (Abee−2)

Fig. 7. Orbital evolution of bolide 2 (Abee-2) in the time span $0 < t < 0.49$ Myr. The lower left-side panels show the semimajor axis a (AU) and eccentricity e vs. time, whereas the other panels show the critical arguments for the ν_2, ν_3, ν_4, ν_5, ν_6 and ν_7 secular resonances.
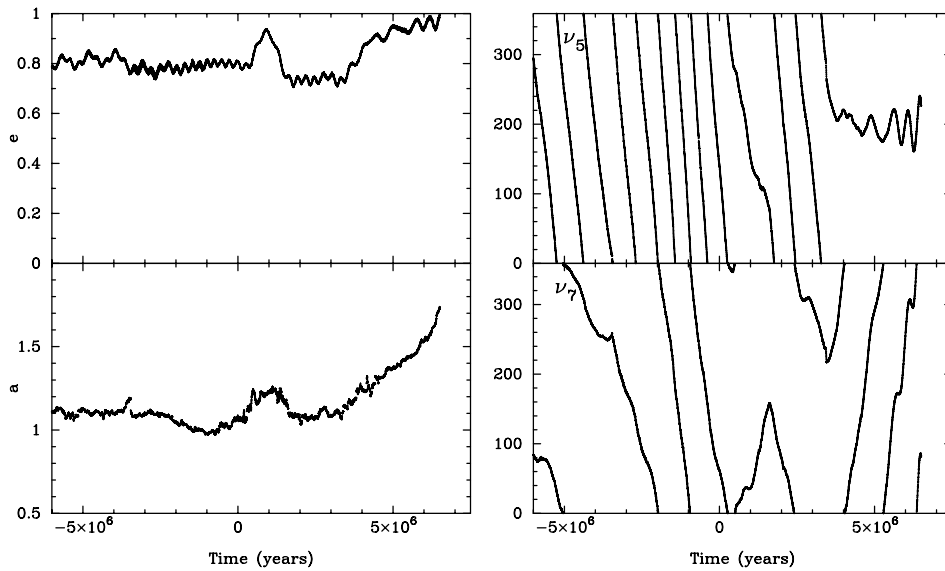
bolide 18 (Tisza)

Fig. 8. Orbital evolution of bolide 18 (Tisza) in the time span $-6 < t < 6.5$ Myr. The left-side panels show the semimajor axis a (AU) and eccentricity e vs. time, whereas the right-side panels show the critical arguments for the ν_5 and ν_7 secular resonances. The ν_5 resonance is clearly responsible for the eventual gradual growth of e up to unity.
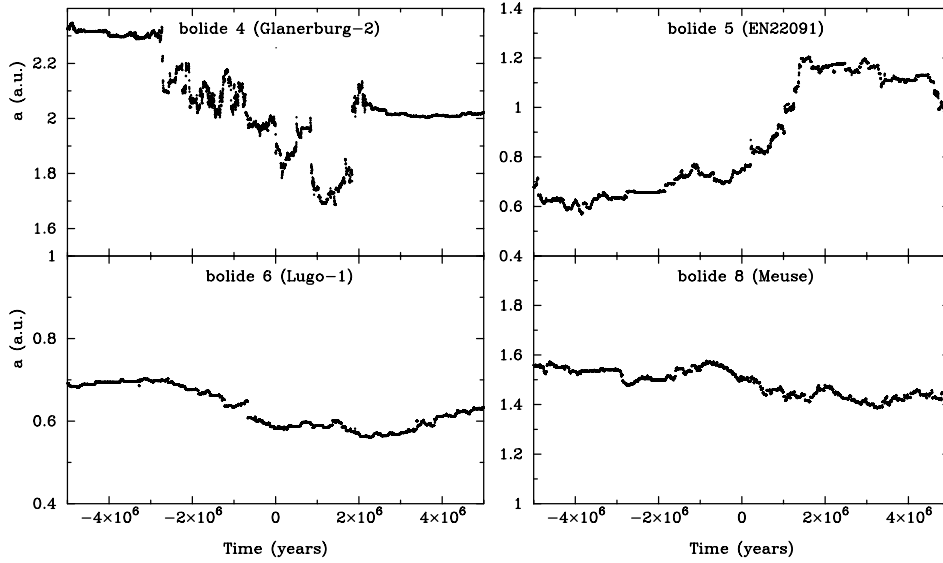
Fig. 9. The semimajor axis evolution of bolides 4, 5, 6 and 8 (Glanerbrug-2, EN220991, Lugo-1 and Meuse, respectively) in the time span $-5 < t < 5$ Myr. The frequent jumps, resulting in a sort of random walk, are caused by planetary close encounters.

Table 5. Osculating elements of the 26 bolides at the common epoch JD 2440000.5. Reference frame: heliocentric, ecliptic 2000.0.

Bolide	T_p JD	q [AU]	e	ω [deg]	Ω [deg]	i [deg]
1	2439816.813671	0.960	0.490	325.0	261.1	1.6
2	2439546.959065	0.977	0.593	325.1	262.0	0.8
3	2439152.402848	0.925	0.723	219.5	17.7	25.0
4	2440113.774018	0.908	0.532	223.0	17.4	21.6
5	2440110.579475	0.468	0.376	17.2	180.2	19.1
6	2439960.323716	0.144	0.753	170.8	119.2	44.3
7	2439906.306483	0.316	0.514	178.5	119.4	23.3
8	2440334.204145	0.651	0.567	267.2	334.2	32.7
9	2439908.540882	0.966	0.518	208.3	136.3	18.8
10	2440143.326386	0.592	0.660	262.7	139.2	1.8
11	2440101.899392	0.561	0.739	260.3	140.2	1.8
12	2440238.214685	0.982	0.580	173.6	327.0	34.0
13	2439861.616352	0.908	0.556	309.1	248.2	2.7
14	2439548.960363	1.016	0.480	182.7	79.9	0.4
15	2440477.151674	0.522	0.781	275.8	33.9	3.9
16	2440228.403482	0.403	0.750	115.5	309.7	4.2
17	2440028.384535	0.569	0.571	280.0	211.3	52.9
18	2439867.268518	0.208	0.807	142.3	29.3	6.0
19	2439948.787046	0.388	0.831	110.6	45.3	5.2
20	2441053.138446	0.714	0.785	235.8	247.6	13.9
21	2439542.141138	0.945	0.667	197.5	295.5	36.8
22	2442706.907383	0.898	0.880	142.5	353.6	8.3
23	2438679.728455	0.506	0.920	259.8	134.9	6.8
24	2439859.238658	0.976	0.088	330.0	60.4	7.1
25	2439985.166766	0.987	0.329	358.6	60.8	15.7
26	2439416.670702	0.983	0.560	3.8	61.1	20.5

Table 6. Estimate of the sensitivity of the numerical integration to the initial coordinates. The Table gives the maximum differences between the final coordinates of the test particles associated to each bolide (Δx, Δy, Δz in AU; $\Delta\dot{x}$, $\Delta\dot{y}$, $\Delta\dot{z}$ in AU/day).

Bol.	Δx	Δy	Δz	$\Delta\dot{x}$	$\Delta\dot{y}$	$\Delta\dot{z}$
1	0.040	0.052	0.001	0.00041	0.00006	0.00001
2	0.005	0.053	0.000	0.00018	0.00008	0.00000
3	0.020	0.066	0.032	0.00011	0.00012	0.00004
4	0.042	0.151	0.052	0.00091	0.00083	0.00042
5	0.229	0.233	0.080	0.00580	0.00367	0.00131
6	0.006	0.008	0.002	0.00002	0.00028	0.00011
7	0.012	0.005	0.006	0.00016	0.00033	0.00000
8	0.035	0.019	0.001	0.00012	0.00021	0.00015
9	0.038	0.037	0.000	0.00012	0.00042	0.00013
10	0.133	0.087	0.006	0.00007	0.00112	0.00003
11	0.118	0.154	0.007	0.00017	0.00142	0.00003
12	0.078	0.078	0.014	0.00047	0.00003	0.00019
13	0.160	0.017	0.006	0.00068	0.00084	0.00004
14	0.038	0.015	0.001	0.00005	0.00020	0.00000
15	0.003	0.015	0.001	0.00005	0.00004	0.00000
16	0.035	0.020	0.003	0.00004	0.00026	0.00001
17	0.071	0.011	0.035	0.00100	0.00131	0.00082
18	0.037	0.021	0.000	0.00050	0.00019	0.00005
19	0.170	0.193	0.024	0.00002	0.00310	0.00020
20	0.081	0.051	0.017	0.00012	0.00018	0.00003
21	0.091	0.046	0.045	0.00010	0.00029	0.00003
22	0.006	0.059	0.010	0.00003	0.00002	0.00000
23	0.088	0.081	0.016	0.00008	0.00004	0.00001
24	0.008	0.020	0.000	0.00030	0.00009	0.00004
25	0.134	0.041	0.039	0.00050	0.00212	0.00017
26	0.064	0.042	0.029	0.00015	0.00029	0.00000

(1997), but only for orbits with $a < 2$ AU. In the present case, it occurs at $a > 2$ AU but has a similar effect, i.e. it pumps up the eccentricity so that after several close encounters e reaches unity (Fig. 6).

Marshall Islands-2 (orbit 11) hits the Sun while its semimajor axis is smaller than 2 AU. In this case the eccentricity is increased up to 1 due to the fact that the body is located in an overlapping region of two secular resonances: the ν_2 and ν_5 resonances, which involve the orbital frequencies of Venus and Jupiter, respectively. The fact that this dynamical mechanism can also lead to a solar collision has recently been pointed out by Gladman et al. (1999).

Table 7. Summary of simulations – Part 1. KLD stands for "Kozai-like dynamics", CE for "close encounter". The time spans over which the different dynamical mechanisms are active are given in brackets, (Myr).

Body	Resonances	Effects	Sun	Ejection	Remarks
1	5/2 Jupiter (−1.14; −0.83)	e ↗~ 1.		−1.14	CE Earth:
	ν_3, ν_4 (−0.4; −0.1)	e.4 ↗.5			2×10^{-4} AU; −0.83 Myr
	ν_6 (+0.4; +1.1)	e.5 ↘.3 ↗.65			→ 5/2 Jupiter
	ν_3, ν_4 (+1.0; +1.49)	e.5 ↗~ 1.			CE Jupiter:
	4/1 Jupiter (+0.8; +1.40)	" "	+1.5		4.8×10^{-2} AU; −1.1 Myr
2	3/1 Jupiter (−0.14; +0.01)	e.4 ↗~ 1.	−0.14		
	ν_6 (+0.0; +0.15)	e.4 ↗.95			
	very close to ν_3, ν_4 (+0.02; +0.3)	e.95 ↘.8 ↗.9			
	ν_2 (+0.38; +0.49)	e.9 ↘.8 ↗~ 1.	+0.49		
	ν_5 (+0.32; +0.49)				
3	2/1 Jupiter (−1.36; +0.15)	chaotic oscill. e ↗~ 1.	−1.36	+0.27	CE Jupiter:
	KLD (−1.36; −1.1)	ω 90			2.3×10^{-2} AU; +0.26 Myr
	ν_5, ν_7 (−0.3; +0.25)	e.6 ↗.9			
	ν_2 alternator (−0.3; +0.25)	e.6 ↗.9			
	KLD (+0.0; +0.25)	ω 180			
4	ν_3, ν_4 (−2.0; −0.5)	e.99 ↘.5			
	ν_3, ν_4 (+2.0; +3.0)	e.35 ↗.7			
5	ν_{13}, ν_{14} (+1.0; +2.0)	i 10. − 20.			
	ν_{13} (+5.0; +6.0)				
6	ν_{13}, ν_{14} (−1.0; +4.0)	e oscill..65 ↗ .9			when out of ν_{13}, ν_{14}
	KLD	ω 0 180			(−5.0; −1.0)
					e oscill..4 −.75
7	ν_{13}, ν_{14} (−5.0; −1.0)				
	ν_{16} (−1.0; +0.1)	e.3 ↗.7; i 30. ↘ 10.			
	KLD (−1.0; +6.0)	ω 0 180			
8	ν_{13}, ν_{14} (−5.; +2.)	coupled oscill. e and i			
	KLD (+4.; +6.)	ω 90 270			
9	3/1 Jupiter (−2.78; −2.30)	$e \sim 1.$ ↘.6	−2.78		
	ν_6 (−1.5; −1.0)	e.5 ↗.7			
	ν_3, ν_4 (+0.0; +0.4)	e.6 ↗.7			
	3/1 Jupiter (+0.8; +1.5)				
	ν_6 (+1.5; +1.7)	e.7 ↗.9			
	ν_2, ν_5 (+1.75; +1.8)	e ↗ 1.			
	8/3 Jupiter(+1.6; +1.8)	e.7 ↗~ 1.		+1.8	
10	ν_3, ν_4 (−0.9; −0.5)	$e \sim 1.$ ↘.6	−0.9		
	KLD (+3.0; +5.47)	ω 0 180			
	ν_3, ν_4 alternator (+3.5; +5.47)	e 0.5 ↗~ 1.	+5.47		

5.2. Forward integrations

As shown in Table 7, in this sample of integrations 12 bodies hit the Sun and 5 are ejected from the solar system. 8 over 17 objects have a lifetime shorter than 1 Myr (5/12 and 3/5, respectively).

While in the backward integration Glanerbrug-1 (3) was driven into the Sun, in the forward one it is ejected outside Saturn's orbit. Fig. 5 shows its evolution. Until $t = 0.19$ Myr it is located in the 2/1 mean motion resonance. Then it leaves the resonance due to a planetary close encounter. During the whole forward integration, it is also temporarily located in the ν_5 and ν_7 secular resonances, the resonant arguments $\varpi - \varpi_5$ and $\varpi - \varpi_7$ alternating between circulation and libration (here ϖ designates the longitude of perihelion). In addition, the orbit is located in the Kozai resonance, the argument of perihelion ω librating around $180°$. Consequently, the eccentricity evolves in a strongly chaotic manner and undergoes large oscillations between 0.4 and 0.9. Then the bolide is ejected outside Saturn's orbit at $t = 0.27$ Myr, following a close encounter with Jupiter.

The inclination of Marshall Islands-2 (11) remains very low during the entire integration timespan, varying between about $2°$ and $5°$. As a consequence, the body suffers frequent planetary close encounters and the eccentricity behaves chaotically, with values ranging between 0.3 and 0.75. Then a close encounter with the Earth injects it in the 3/1 resonance, where its eccentricity oscillates between 0.6 and 0.9. Finally, a close approach to Jupiter ejects the bolide outside Saturn's orbit at $t = 0.81$ Myr.

Like in the backward integration, the comet-like bolide EN270796 (23) is ejected after only 0.19 Myr by a close encounter with Jupiter. This short lifetime is quite typical for short-period comets (see e.g. Levison & Duncan 1994).

Table 8. Summary of simulations – Part 2.

Body	Resonances	Effects	Sun	Ejection	Remarks
11	ν_2, ν_5 (−1.07; −0.7)	$e \sim 1.$ ↘.8	−1.07		CE Jupiter:
	ν_3, ν_4 (−0.5; 0.0)	e.7 ↘.4			4.3×10^{-2} AU; +0.81 Myr
	3/1 Jupiter (0.4; 0.81)	chaotic e ↗~ 1.		+0.81	
12	3/1 Jupiter (−5.5; −5.0)	e.6 ↗.98 ↘.6			KLD
		i 20. ↗ 75. ↘ 20.			
	ν_2, ν_5 (−5.0; −4.0)	" "			.5 < e < .8
	ν_3, ν_4 (−0.5; +0.5)				20. < i < 50.
	ν_6 (+0.5; +1.0)	e.6 ↗ ~ 1.	+1.1		
	3/1 Jupiter (+0.6; +0.8)	e.8 ↘.4 ↗.8			
13	ν_6 (−3.24; −3.0)	$e \sim 1.$ ↘.5	−3.24		
	4/1 Jupiter (−2.0; +0.0)	e oscill..2 −.5			
	ν_6 (−0.5; +0.0)	e.1 ↗.7			
	ν_3, ν_4 (+0.0; +2.0)	e.4 ↗.5			
	ν_2 (+2.7; +3.2)				
	ν_5, ν_7 (+3.0; +4.0)	e.4 ↗.55			
14	ν_5, ν_7 (−7.0; −6.0)	e.4 ↘.3			CE Jupiter:
	ν_3, ν_4 (+1.0; +2.0)				3.6×10^{-2} AU; +3.53 Myr
	ν_3, ν_4 (+2.5; +3.5)	e.5 ↗.9		+3.53	
15	4/1 Jupiter, ν_2, ν_5 (−2.46; −2.20)	$e \sim 1.$ ↘.8	−2.46		
	ν_6 (−2.1; −2.0)	e.8 ↘.5			
	ν_6 (−0.8; −0.6)	e.5 ↗.7			
	ν_6 (+0.1; +0.3)	e.7 ↗.8			
	3/5 Mars, ν_2, ν_5 (+0.3; +0.34)	e 0.8 ↗~ 1.		+0.34	
16	ν_2 (−6.0; −5.0)	e oscill..6 −.85			
	ν_2 (−4.0; −2.0)	" "			
	ν_5, ν_7 (+2.0; +2.7)	e.55 ↗ ~ 1.		+2.7	
17	KLD (−8.0; +5.0)	ω 270			
	ν_{16} (−8.0; +0.0)	large coupled oscill. e/i			
18	ν_7 (+0.0; +4.0)	e.8 ↗.95 ↘.8			
	ν_5 (+4.0; +6.5)	e.8 ↗~ 1.		+6.5	
19	ν_6 (−0.26; +0.2)	e.8 ↗ ~ 1.	−0.26		
	3/1 Jupiter (−0.26; −0.17)	$e \sim 1.$ ↘.65			
	ν_3, ν_4 (−0.08; +0.12)	e.8 ↗~ 1.		+0.12	
20	2/1 Jupiter (−0.87; +0.0)	e oscill. $\sim 1.$ ↘.2		−0.87	CE Jupiter:
	ν_2, ν_5, ν_7 (−0.7; −0.5)	e.6 ↘.4			4.4×10^{-2} AU; −0.82 Myr
	ν_2, ν_5, ν_7 (+0.0; +0.06)	e.6 ↗~ 1.		+0.06	

The case of St. Roberts (14) is quite unusual. Since its inclination is very small, it suffers numerous close approaches, especially with Mars. Moreover, between $t = 1$ Myr and 3.5 Myr it is located in the overlapping region of the ν_3 and ν_4 secular resonances, and its eccentricity increases from 0.5 to 0.9. At this time, although the semimajor axis is approximately 1.8 AU, it undergoes a sequence of very close encounters with both Venus and Mars, which eventually eject it from the Solar System.

It is worthwhile noting that among the 12 solar collisions which have been detected, 7 are caused by dynamical mechanisms which involve secular resonances. For 5 bodies, the solar collision occurs when their semimajor axis is > 2 AU.

As shown in Fig. 7, the orbital evolution of Abee-2 (2) is affected by secular resonances with both the terrestrial and the giant planets during the entire forward integration timespan. The eccentricity at first is increased as an effect of ν_6, then due to both ν_3 and ν_4. Finally, the body enters the region where ν_2, ν_5 and ν_7 are active so that the eccentricity is pumped up to unity. Note that the eccentricity increase is quite regular and its oscillations are coupled with those of the resonant arguments. A similar behaviour is found for EN081195B (19). However, its initial eccentricity is already 0.83, and the orbit lies in both ν_3 and ν_4 during the whole forward integration. Then, the eccentricity increases up to 1 in a regular manner.

Since its inclination is relatively small, Marshall Islands-1 (10) undergoes many close encounters with Mars and the Earth. The evolutions of the semimajor axis and eccentricity are thus correlated during the first 3 Myr. Then the body undergoes some Kozai-like dynamics — the oscillations of the eccentricity becoming larger, with an amplitude $\simeq 0.25$ — and is also temporarily located in ν_3 and ν_4, the corresponding resonant arguments alternating between libration and circulation; consequently, the eccentricity is secularly increased up to unity within 2.4 Myr.

As indicated in Table 7, the eccentricity of Dresden (12) is first increased up to 0.7 as an effect of ν_3 and ν_4; then the orbit

Table 9. Summary of simulations – Part 3.

Body	Resonances	Effects	Sun	Ejection	Remarks
21	ν_2, ν_5, ν_7 $(-0.19; 0)$	chaotic e	-0.19		
	5/2 Jupiter $(-0.10; +1.20)$	$e \sim 1. \searrow .4$			
	ν_3, ν_4 $(-0.05; +0.20)$	" "			
	ν_3, ν_4 alternator $(+1.0; +1.45)$				
	3/1 Jupiter $(+1.6; +2.0)$	$e.7 \nearrow \sim 1. \searrow .7$			
	ν_2, ν_5, ν_7 $(+1.6; +2.38)$	$e.7 \nearrow \sim 1.$	$+2.38$		
22				-0.10	CE Jupiter 4×10^{-3} AU
			$+0.012$		CE Jupiter 5×10^{-3} AU
23				-0.04	CE Jupiter 1×10^{-4} AU
				$+0.19$	CE Jupiter 5×10^{-3} AU
24	7/1 Jupiter $(-5.0; -0.5)$	e oscill. $0. -.2$			
	ν_3, ν_4 $(-5.0; -4.0)$	" "			
	ν_3, ν_4 $(-3.0; -2.0)$	" "			
	ν_5 $(-2.0; -1.0)$	" "			
	ν_{13}, ν_{14} alternator $(-5.0; +0.0)$	i oscill. $0. - 20.$			
25	ν_{13}, ν_{14} alternator $(-4.5; -1.5)$				
	ν_{13}, ν_{14} $(+0.5; +2.0)$				
26	4/1 Jupiter, ν_2, ν_5 $(-5.01; -4.7)$	$e \sim 1. \searrow .7$	-5.01		
	ν_3, ν_4 $(-4.8; -4.2)$				
	ν_6 $(-4.5; -2.5)$	$e\,0.6 \searrow .16 \nearrow .7$			CE Earth:
	ν_3, ν_4 $(-2.5; -1.0)$	$e.6 \nearrow .8$			3×10^{-4} AU; $+1.27$ Myr
	ν_6 $(+0.0; +1.2)$	$e\,0.7 \searrow .3 \nearrow .8$			CE Jupiter:
	1/6 Venus $(+0.7; +1.0)$	$e.4 \nearrow .9$		$+1.3$	3.4×10^{-2} AU; $+1.3$ Myr
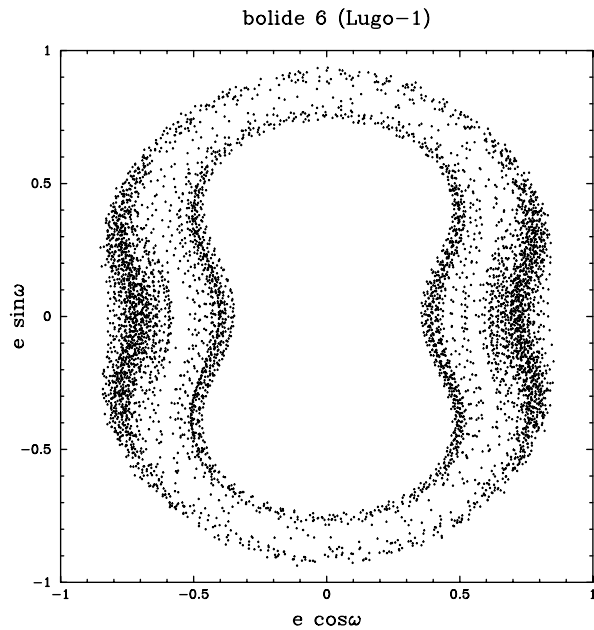
bolide 6 (Lugo-1)

Fig. 10. Evolution in the $e \sin \omega$ vs. $e \cos \omega$ plane of the orbit of bolide 6 (Lugo-1). This pattern is typical of Kozai-like dynamics.

enters ν_6, which pumps its eccentricity up to 1 within 0.5 Myr, causing a collision with the Sun.

Two other bolides have a collision with the Sun when their semimajor axes are < 2 AU. Žamberk (16) and Tisza (18) have semimajor axes between 1.2 and 1.6 AU. They become Sun-grazing due to their location in the ν_5 secular resonance (Fig. 8).

As already noted, this new *route* to the Sun has been recently identified by Gladman et al. (1999).

Since the Dobříš II (22) collides with the Sun only after 0.012 Myr, we have been unable to detect any specific transport mechanism. However, its initial conditions imply that this orbit is clearly of a comet-like type.

The dynamical evolution of the last four bodies, namely Abee-1 (1), Polná (9), Kouřim (15) and Ózd (21), are affected by both mean motion and secular resonances, as indicated in Table 7. As a result, the evolution of their eccentricity is strongly chaotic. All of them hit the Sun when their semimajor axis is larger than 2 AU.

5.3. Orbits dominated by close approaches

Seven orbits (4, 5, 6, 7, 8, 24, 25) have their semimajor axis strongly affected by close planetary encounters. Indeed, as illustrated in Fig. 9, this parameter undergoes a sort of random walk due to frequent planetary close approaches, both shallow and deep ones. Moreover, six orbits (5, 6, 7, 8, 24, 25), which over the whole integration time (at least 10 Myr) have a semimajor axis < 1.7 AU, are temporarily located in the region where the ν_{13} and ν_{14} nodal secular resonances overlap, causing increases of the inclination. Kozai dynamics is observed for orbits 6, 7, 8 (see Table 7), either temporarily or during the entire timespan (see e.g. Fig. 10). In this regime, the orbits are often protected from close approaches, and therefore their lifetime is lengthened.

Let us consider now the evolution of these orbits in the a–e plane. During the entire integration time, bolide Honduras-1
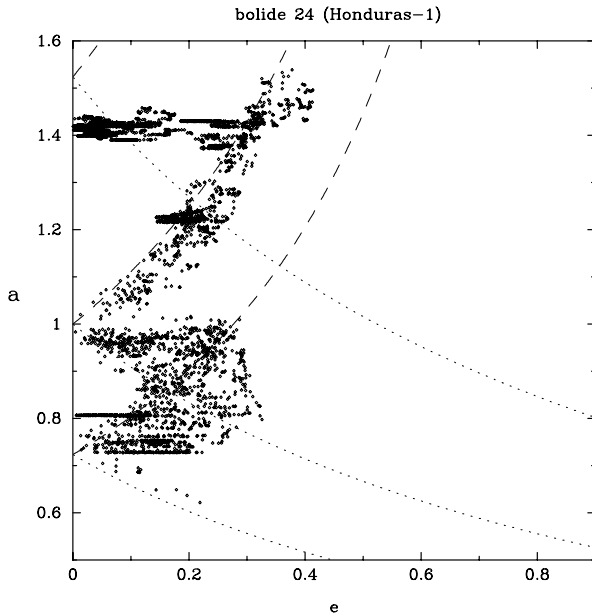
Fig. 11. Orbital evolution of bolide 24 (Honduras-1) in the semimajor axis vs. eccentricity plane over the $-5 < t < 5$ Myr time span. Dashed and dotted curves correspond to orbits having perihelia and aphelia nearly tangent to the orbits of Mars, the Earth and Venus. While secular resonances at times affect the eccentricity (causing horizontal displacements in this diagram), close encounters with the Earth and Venus move the orbit roughly along lines of constant perihelion or aphelion distance (Michel et al. 1996b), bringing it through the Amor, Apollo, Aten and $Q < 1$ AU regions.

(24) crosses all the region of near-Earth space, being temporarily a ($Q < 1$ AU), Aten ($a < 1$ U, $Q > 1$ AU), Apollo and Amor-like body (Fig. 11). In the backward integration ($-5 \leq t \leq -0.5$ Myr), it is an Amor body with a semimajor axis always larger than 1 AU, and an eccentricity smaller than 0.2. Then it becomes an Apollo, i.e. its trajectory crosses Earth's orbit. Between 0.5 Myr and 2.5 Myr, it enters the region with $Q < 1$ AU, defined as the region with $a < 1$ AU and aphelion distance $Q < 0.983$ AU, and alternates several times between the $Q < 1$ AU and Aten states. Finally it goes back in a Apollo-like orbit and then into the Amor region. This evolution shows nicely the continuous interchange, over a time scale of several Myr, among the different sub-populations of near-Earth objects.

A similar behaviour is found in other cases (see Figs. 12 and 13). Bolide Lugo (6, 7), for which 2 different orbits have been integrated, is always a body with $Q < 1$ AU or an Aten body (i.e. its semimajor axis is always < 1 AU), entering and exiting several times into/from the two regions. Between $t = -5$ Myr and $t = +1$ Myr, the orbit of bolide 5 interchanges several times between the $Q < 1$ AU and Aten states. Then its semimajor axis becomes > 1 AU and it becomes an Apollo. Finally, it re-enters the Aten region at $t \simeq 5.6$ Myr. On the other hand, the orbits of bolides 4 and 8 show the same behaviour but in the Amor/Apollo regions. As for bolide 25, it keeps always a semimajor axis $a > 1$ AU and thus remains an Apollo during almost all the integration time, but it makes short visits into the

Amor region. Fig. 13 shows that its evolution occurs close to the $q = 1$ AU curve, as expected for a body whose evolution is dominated by Earth encounters.

6. Conclusions

The main conclusions from this work can be summarized as follows.

1. We confirm the conclusion by Jopek et al. (1995) that a great variety of orbital parameters and evolutions is found in the bolide population, quite comparable to that observed for the larger near-Earth objects. The main dynamical mechanisms affecting the orbits are mean motion and secular resonances (frequently overlapping each other) and close planetary encounters. This results in very chaotic evolutions, with dynamical lifetimes which can be as short as $\approx 10^5$ or as long as $> 10^7$ yr.

2. The most frequent fates of these bodies are solar collision and ejection into a hyperbolic orbit. We have integrated 52 orbits (26 backward and 26 forward in time) and have found 22/52 solar collisions (42%) and 9/52 ejections (17%). These percentages are very similar to those found for the near-Earth object population over a 60 Myr time span by Gladman et al. (1999), and the same holds for the average median lifetimes which can be inferred from our data, of the order of 10 Myr. On the other hand, some specific orbits evolve only slowly, and they probably account for a tail of long-lived bodies for which collisions are probably the dominant lifetime-limiting process.

3. We have only two clearly comet-like sets of initial orbital elements in our sample of starting orbits, although four bodies were classified in Ceplecha's physical "cometary" group. While our sample is probably biased by selection effects (which typically favour "meteoritic" bolides against "cometary" ones) and while there are dynamical pathways between cometary (Jupiter-coupled) and asteroidal orbits, our results provide some support to the idea that only a minor fraction (possibly 10–20%) of the near-Earth population would be of cometary origin. For km-sized near-Earth objects, convincing evidence for this conclusion comes from spectroscopic and rotational studies (McFadden et al. 1989, Lupishko & Di Martino 1998, Binzel et al. 1992). On the other hand, the predominance of the asteroidal component in the 1–10 m size range (especially near its upper end) is at odds with Ceplecha's (1994, Ceplecha et al., 1997) finding that very weak, "cometary" bodies are very frequent in the bolide population at these sizes. A possibility to solve this conundrum is that asteroids might also supply to the Earth very fragile and/or porous material (see e.g. Foschini 1998).

4. We have found that among the 8 encounter-dominated orbits, four, the two corresponding to the Lugo bolide (6, 7) plus EN220991 (5) and Honduras-1 (24), are initially or become temporarily later Aten-like or bodies with $Q < 1$ AU. This is quite comparable to the observed abundance of such orbits in the near-Earth object population (Michel et al. 1999).
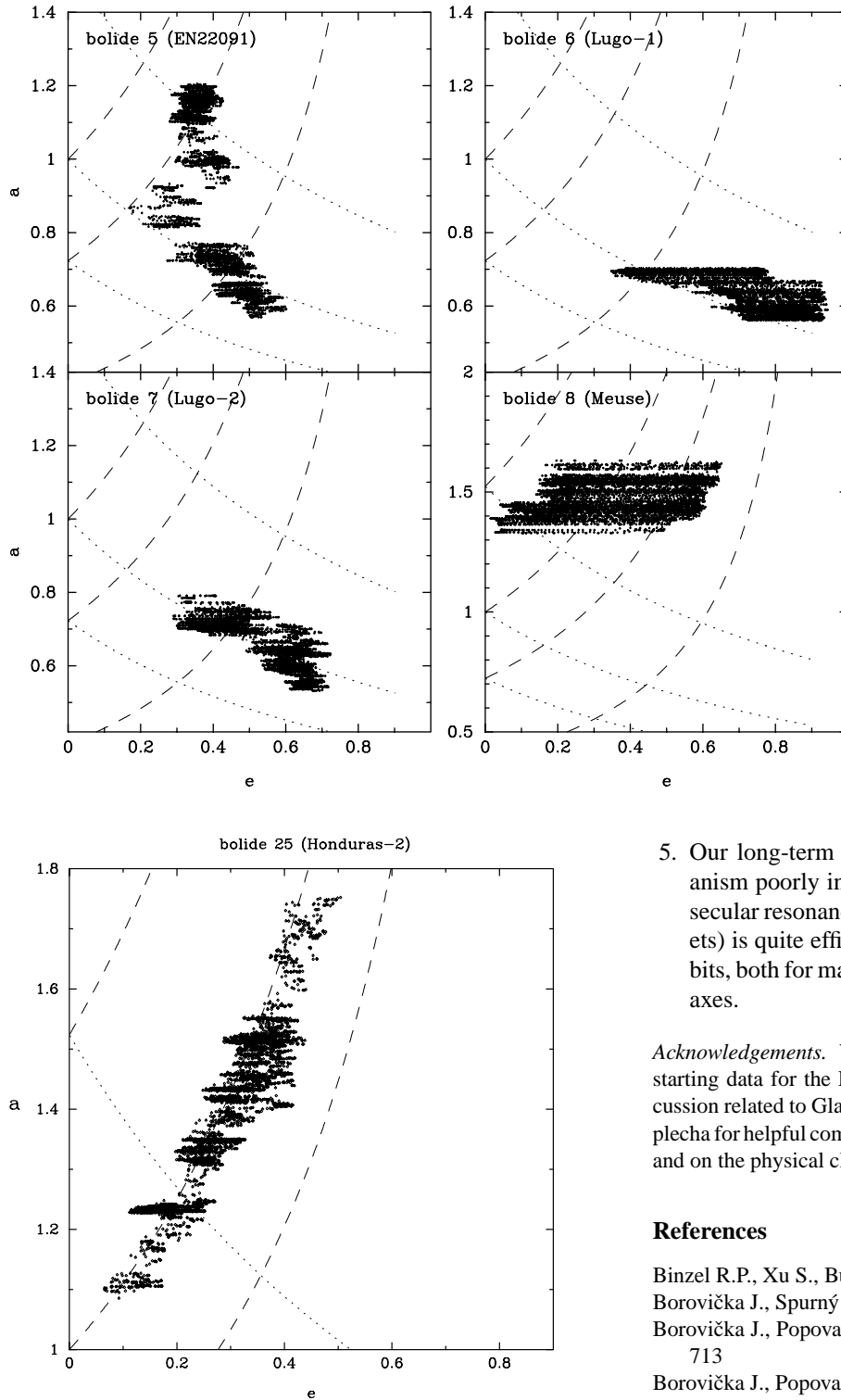
Fig. 12. Orbital evolution in the semimajor axis vs. eccentricity plane of bolides 5, 6, 7 and 8 (EN220991, Lugo-1, Lugo-2 and Meuse, respectively), throughout the 10 Myr integation time span. Dashed and dotted curves correspond to orbits having perihelia and aphelia nearly tangent to the orbits of Mars, the Earth, Venus and Mercury. These orbits are affected by both resonances, which shift them horizontally, and close encounters, which move them near the lines of constant perihelion or aphelion distance. Thanks to the interplay of these two mechanisms, they wander through different regions of the a–e plane.

5. Our long-term integrations show that a dynamical mechanism poorly investigated so far, that is the overlapping of secular resonances (included those involving the inner planets) is quite efficient to transport bodies to Sun-grazing orbits, both for main-belt (> 2 AU) and for smaller semimajor axes.
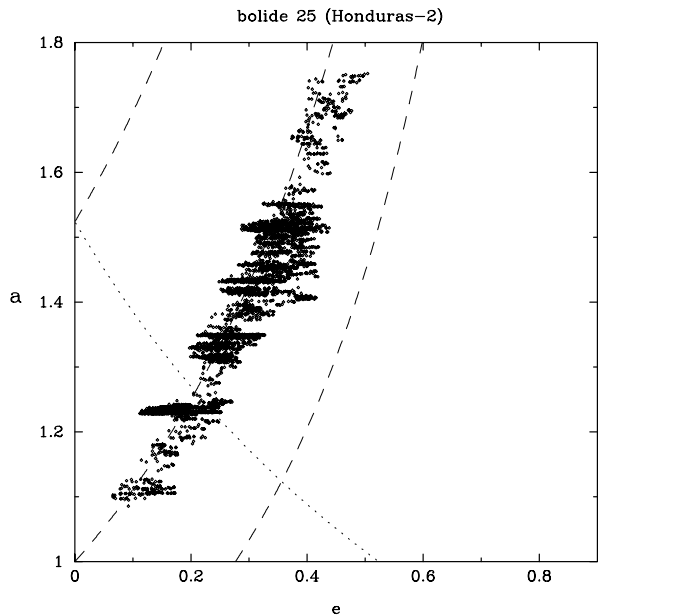
Fig. 13. Orbital evolution of bolide 25 (Honduras-2) in the a–e plane during the 10-Myr integration time span. Dashed and dotted curves correspond to orbits having perihelia and aphelia nearly tangent to the orbits of Mars, the Earth and Venus. The dominant role of Earth close encounters is apparent as the orbit keeps its perihelion distance close to 1 AU.

References

Binzel R.P., Xu S., Bus S.J., et al., 1992, Science 257, 779

Borovička J., Spurný P., 1998, Říše hvězd, 73, 124

Borovička J., Popova O.P., Nemtchinov I.V., et al., 1998a, A&A 334, 713

Borovička J., Popova O.P., Golub' A.P., et al., 1998b, A&A 337, 591

Borovička J., Pineda de Carias M.C., Ocampo A., et al., 1999, in: Meteoroids 1998, ed. V. Porubčan, Slovak Acad. Sci., submitted

Brown P., Hildebrand A.R., Green D.W.E., et al., 1996, Meteorit. Planet. Sci. 31, 502

Ceplecha Z., 1994, A&A 286, 967

Ceplecha Z., 1995, Earth, Moon, Planets 68, 107

Ceplecha Z., 1999, in: Meteoroids 1998, ed. V. Porubčan, Slovak Acad. Sci., submitted

Ceplecha Z., McCrosky R.E., 1976, J. Geophys. Res. 81, 6257

Ceplecha Z., Spurný P., Borovička J., et al., 1993, A&A 279, 615

Ceplecha Z., Jacobs C., Zaffery C., 1997, Annals New York Academy of Sciences 822, 145.

Cevolani G., Foschini L., Trivellone G., 1993, Nuovo Cimento 16C, 463

Cevolani G., Hajduková M., Foschini L., et al., 1994, Contrib. Astron. Obs. Skalnaté Pleso 24, 117

Chyba C.F., Thomas P.J., Zahnle K.J., 1993, Nature 361, 40

Farinella P., Froeschlé C., Gonczi R., 1994, in: Proc. IAU Symp. 160 – Asteroids, Comets, Meteors 1993, eds. A. Milani, M. Di Martino, A. Cellino, Kluwer, Dordrecht, p. 205

Farinella P., Vokroulický D., Hartmann W.K., 1998, Icarus 132, 378

Foschini L., 1998, A&A 337, L5

Foschini L., 1999, A&A 342, L1

Gaffey M.J., Reed K.L., Kelley M.S., 1992, Icarus 100, 95

Gladman B., Michel P., Froeschlé Ch., 1999, Icarus, submitted

Griffin A.A., Millman P.M., Halliday I., 1992, J. Roy. Astron. Soc. Can. 86, 5

Halliday I., Griffin A.A., Blackwell A.T., 1996, Meteoritics Planet. Sci. 31, 185

Hills J.G., Goda M.P., 1993, AJ 105, 1114

Jenniskens P., Borovička J., Betlem H., et al., 1992, A&A 255, 373

Jopek T.J., Farinella P., Froeschlé Ch., et al., 1995, A&A 302, 290; erratum 1996, A&A 314, 353

Levison H., Duncan M., 1994, Icarus 108, 18

Lupishko D.F., Di Martino M., 1998, Planet. Space Sci. 46, 47

Lyne J.E., Tauber M., Fought R., 1996, J. Geophys. Res. 101, 23207

McFadden L.-A., Tholen D.J., Veeder G.J., 1989, in: Asteroids II, eds. R.P. Binzel, T. Gehrels, M.S. Matthews, University of Arizona Press, Tucson, p. 442

Michel P., 1997, Icarus 129, 348

Michel P., Froeschlé Ch., Farinella P., 1996a, A&A 313, 993

Michel P., Froeschlé Ch., Farinella P., 1996b, Earth, Moon, Planets 72, 151

Michel P., Zappalà V., Cellino A., et al., 1999, Icarus, accepted

Migliorini F., Michel P., Morbidelli A., et al., 1998, Science 281, 2022

Moons M., Morbidelli A., 1995, Icarus 114, 33

Morbidelli A., Moons M., 1993, Icarus 102, 316

Morbidelli A., Gladman B., 1998, Meteorit. Planet. Sci. 33, 999

Spurný P., 1997, Planet. Space Sci. 45, 541

Spurný P., Borovička J., 1997, WGN – J. IMO 25, 94

Stoer J., Bulirsch R., 1980, Introduction to Numerical Analysis, Springer, New York

Tagliaferri E., Spalding R., Jacobs C., et al., 1994, in: Hazards Due to Comets and Asteroids, ed. T. Gehrels, University of Arizona Press, Tucson, p. 199

Tagliaferri E., Spalding R., Jacobs C., et al., 1995, Earth, Moon, Planets 68, 563

Valsecchi G.B., Morbidelli A., Gonczi R., et al., 1995, Icarus 118, 169

Vokrouhlický D., Farinella P., 1998, A&A 335, 351

Wetherill G.W., 1967, J. Geophys. Res. 72, 2429

Wetherill G.W., ReVelle D.O., 1981, Icarus 48, 308

Whipple F.L., 1938, Proc. Am. Phil. Soc. 79, 499

Yeomans D.K., Barriot J.B., Dunham D.W., et al., 1997, Science 278, 2106